In Situ Investigation on the Formation Mechanism of MCM-41 Mesoporous Silica by Microcalorimetry

Zhaodong Nan,*,† Meiyun Wang,‡ and Bianqing Yan†

College of Chemistry and Chemical Engineering, Yangzhou University, Yangzhou 225002, China, and College of Chemical Science, Qufu Normal University, Qufu 273165, China

A microcalorimeter was used to investigate the formation mechanism of MCM-41 mesoporous silica. The obtained results show that the formation processes of the sample contain three steps. On the basis of the calorimetric results, MCM-41 mesoporous silica was successfully synthesized under basic conditions at different experimental times, such as (1, 2, and 4) h, respectively. Associated with other analytical techniques, the formation mechanism of the produced silica is proposed. First, rodlike inorganic/surfactant complexes are formed which spontaneously pack into an ordered arrangement. Second, with the help of this new template, a new kind of pore structure is formed. Third, the interaction between the pore structures formed in steps 1 and 2 results in a new pore structure. This new pore structure is very similar to the structure formed in the first step. The present work proves that calorimetry can be used for investigations on the formation mechanism of materials.

Introduction

Mesoporous silica has received much attention because of its wide application from which it was first discovered by working for Mobil Oil Group.[1,2] The formation mechanism of mesoporous silicas has been investigated by many researchers. A liquid crystal templating mechanism was first employed to explain the development of uniform mesopores,[1] and then a cooperative templating mechanism.[3,4] In situ X-ray diffraction (XRD) measurements, using a synchrotron beam, revealed two stages in the formation of MCM-41: the long-range order is completed within 3 min, and from then on only silica condensation occurs.[5,6] The IR technique was used to investigate the formation process of mesoporous materials. The results showed that the ordering of the surfactant molecules increases during the reaction.[7] The formation process of MCM-41 under acidic conditions was examined by grazing incident synchrotron radiation diffraction.[8,9] Two steps were identified: the first is referred to as an induction period during which ordering of the silicate and surfactant molecules at the interface occurs, and at the end of this stage, a diffraction pattern is developed. This is then followed by a rapid growth of a layered structure. For in situ EPR measurements, two clear stages were also found: a fast one (about 12 min), which is attributed to the formation of a long-range ordered silicate−surfactant mesophase, and a slower one (> 1 h), which is devoted primarily to the completion of the silicate polymerization.[10−12] Cryo-TEM and laser scattering measurements were also carried out to investigate particle growth.[13,14] However, because the mesoporous silicas are produced under various reaction conditions, no single mechanism can be employed to interpret the nucleation, the growth of the particles, and the development of uniform mesopores. These studies clearly showed that techniques permitting in situ investigations of the reaction systems were necessary to get a better insight into the formation processes of mesoporous materials.[15,16]

The techniques for investigation on the formation mechanism of mesoporous materials have not enclosed calorimetry as far as we know. Hydration of MCM-41 has been studied by sorption calorimetry.[17] Can calorimetry be used to investigate the formation processes of mesoporous materials? Calorimety permits in situ measurement of the heat production during the reaction processes without disrupting the system, and the results give qualitative and quantitative indicators to inform us about the changes of the reaction system.

Here, calorimetry has been used to measure the released thermal energy in the processes of forming mesoporous materials. Novel processes were discovered during the formation of mesoporous materials by using the obtained power−time curves.

Experimental

Tetraethoxysilane analytical grade reagent, which contained a mass fraction of 28.0 % SiO_2, was obtained from Tianjing Kemiou Chemical Reagent Co. Solid cetyltrimethylammonium bromide (CTAB) was an analytical grade reagent from Shanghai Ruijie Chemical Reagent Co. Aqueous ammonia, which contained a mass fraction of 26.5 % NH_3, was obtained from Laiyang Shuanghua Co.

In a typical synthesis, a mixture of CTAB, deionized water, and aqueous ammonia was vigorously stirred until a transparent solution was obtained. Tetraethoxysilane (TEOS) was then added slowly dropwise to the solution. The emulsion was regularly stirred for different times, such as (1, 2, and 4) h, respectively, at 298 K. The as-synthesized samples were named as S1, S2, and S3 for the experimental time of (1, 2, and 4) h, respectively. The mole ratio of CTAB:TEOS:NH_3:H_2O was 1:5:100:4000. The solid product was recovered by filtration, washed with distilled water, and dried at room temperature. The mixed surfactants were removed by calcination at 873 K for 6 h. The names of the calcined samples were given as S4, S5, and S6 corresponding to S1, S2, and S3, respectively.

* Corresponding author. Phone: +86-514-87959896. Fax: +86-514-87959896. E-mail: zdnan@yzu.edu.cn.
† Yangzhou University.
‡ Qufu Normal University.

10.1021/je8006502 CCC: $40.75
Published on Web 12/01/2008

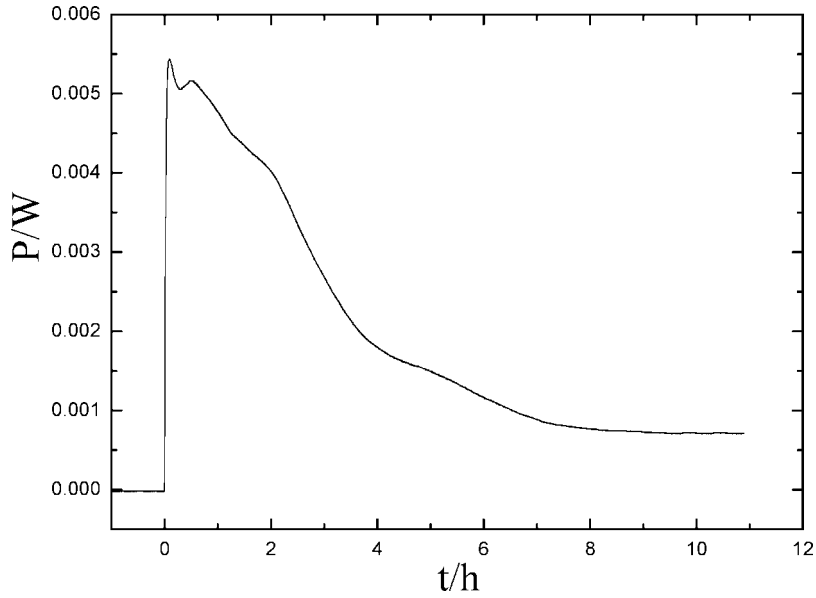

Figure 1. Total power−time curve during the formation processes of the mesoporous SiO_2.

The calorimeter was an eight-channel TAM Air isothermal heat conduction calorimeter 3114/3236 (Thermometric AB, Sweden). The calorimetric channels were in a single removable block contained in an air thermostat that kept the temperature within ± 0.02 K. The limit of detection is 2 μW, and the baseline deviation over 24 h is ± 5 μW. All the calorimetric measurements were performed at (298.15 ± 0.02) K. In the calorimetric experiment, 9.71 mL of the obtained solution containing CTAB and ammonia was placed in an ampule, and 0.15 mL of TEOS was placed in the injector, respectively. Once the baseline was stabilized, the TEOS was injected into the ampule. At the same time, a power−time curve of the reaction was recorded. The mole ratio of CTAB:TEOS:NH_3:H_2O was 1:5:100:4000, which was the same as in the compositions as the synthesized mesoporous silica sample. The re-establishment of a stable baseline indicated that the reaction was complete. All experimental data were calculated by use of the Picolog software supplied with TAM Air.

The enthalpy of dilution of the TEOS was obtained by using 9.71 mL of deionized water to replace the CTAB and ammonia solution in the ampule. The enthalpy of dilution of the CTAB and ammonia solution was obtained by using 0.15 mL of deionized water to replace the TEOS in the injector.

Powder small-angle X-ray diffraction (SXRD) data were obtained on a D/max-rB model with a Cu target at 40 kV and 120 mA, using a speed of 0.2°·min^{-1} and a step of 0.01°.

The morphologies of the as-prepared products were observed by transmission electron microscope (TEM) images, which were taken on a Hitachi model H-800.

Nitrogen adsorption−desorption measurements were carried out on an Omnisorp 100 CX gas adsorption analyzer from Coulter Co. Every sample was degassed at 350 °C for 12 h under a pressure of 10^{-5} Pa or below.

The thermogravimetry (TG) measurements of the samples were carried out by a thermogravimetric analysis system (model: TG 209 F1, NETZSSCH, Germany) under nitrogen with 10 K·min^{-1} heating rate. The amounts of the samples used for TG analysis were (28.9, 29.3, and 29.1) mg, respectively, for S1, S2, and S3. The flow rate of nitrogen for each of TG experiments was controlled at 10 mL·min^{-1}.

Results and Discussion

Figure 1 shows the power−time curve in the total processes during the formation of the mesoporous silica. The power−time curves show highly reproducibility under the same conditions. The total processes contain different steps, such as the reaction step and the diluting steps of TEOS, CTAB, and ammonia, respectively. To get the heat of the reaction step for the formation of mesoporous silica, the heat of diluting reactants should be removed from the obtained total heat. The power−time curve of the diluting TEOS is shown in Figure 2. The heat of the dilution of CTAB and ammonia solution is so small that the diluting steps are ignored. The power−time curve of the formation mesoporous silica is shown in Figure 3, which was gotten by subtracting the power data obtained in Figure 2 from the corresponding power data obtained in Figure 1.

Three exothermic peaks are found from Figure 3. These peaks were separated, and the corresponding enthalpies were calculated as shown in Scheme 1, where h, h_1, and h_2 are the power at time t_1 corresponding to the total curve, "peak 1", and "peak 2", respectively and $h = h_1 + h_2$. The values for h, h_1, and h_2 are about 0.0042 W, 0.0009 W, and 0.0033 W, respectively. The enthalpy changes corresponding to peak 1, peak 2, and peak 3 were calculated by the area ratio as the following equations

$$S_{\mathrm{I}}:S_{\mathrm{II}}:S_{\mathrm{III}} = \Delta H_{\mathrm{I}}:\Delta H_{\mathrm{II}}:\Delta H_{\mathrm{III}} \quad (1)$$

$$\Delta H_{\mathrm{I}} + \Delta H_{\mathrm{II}} + \Delta H_{\mathrm{III}} = \Delta H_{\mathrm{total}} \quad (2)$$

where S_{I}, S_{II}, and S_{III} are areas corresponding to peak 1, peak 2, and peak 3 as shown in Scheme 1, respectively. ΔH_{I}, ΔH_{II}, and ΔH_{III} are enthalpy changes corresponding to peak 1, peak 2, and peak 3, respectively. $\Delta H_{\mathrm{total}}$ is the total enthalpy change during the reaction process. The value of $\Delta H_{\mathrm{total}}$ can be determined by the calorimeter. S_{I}, S_{II}, and S_{III} were obtained from the area of the three parts. Thus, ΔH_{I}, ΔH_{II}, and ΔH_{III} were obtained. The enthalpy values to these peaks are given in Table 1, and other results are given in the Supporting Information.

Three mesoporous silica samples were synthesized based on the different steps. The morphologies of the samples were examined by TEM. Figure 4 shows TEM photos of the obtained samples with different experimental times. The synthesized

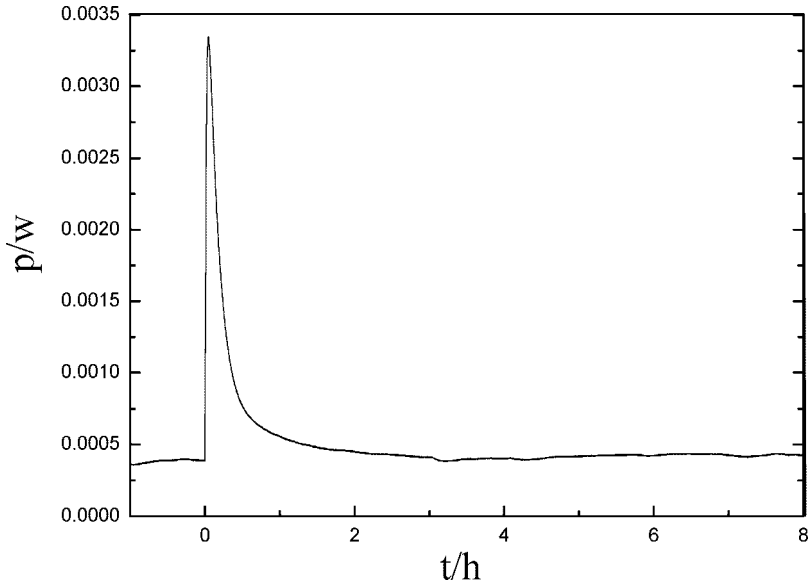

Figure 2. Power−time curve of the dilution of TEOS.

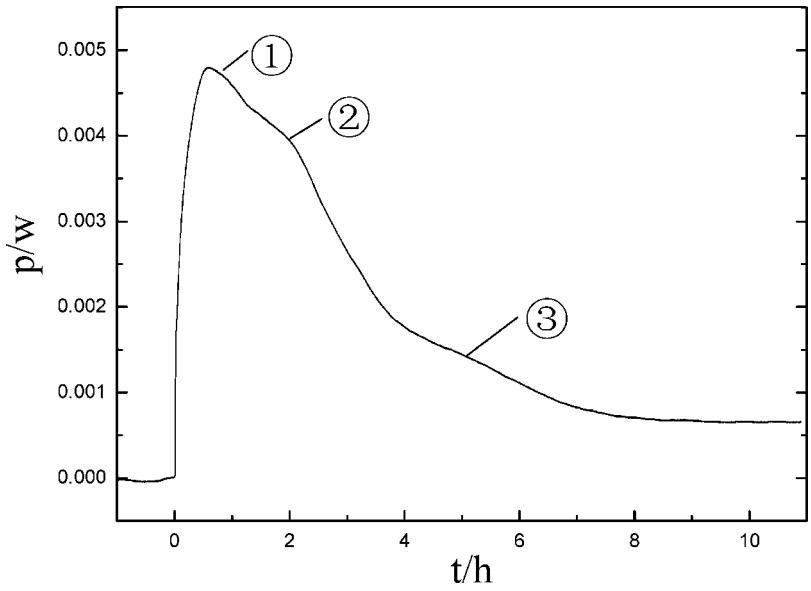

Figure 3. Power−time curve of the reaction during the formation processes of the mesoporous silica.

Scheme 1. Separation of the Power−Time Curve and Calculation of the Enthalpy for the Processes

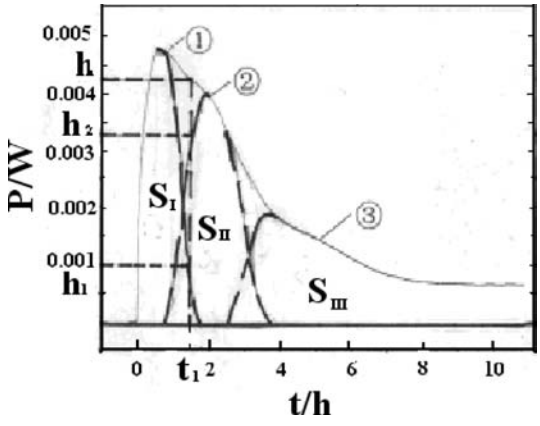

samples all give rodlike morphologies. The results prove that the samples do not change significantly in morphology with the change of the experimental time.

Table 1. Enthalpy during the Processes of Formation of Mesoporous Silica

total enthalpy/J	enthalpy of peak 1/J	enthalpy of peak 2/J	enthalpy of peak 3/J
47.6 ± 0.4	7.1 ± 0.3	24.5 ± 0.5	16.0 ± 0.5

SXRD patterns of the as-synthesized samples are shown in Figures 5 and 6, respectively. An intense diffraction (100) peak at about $2\theta = 2°$ and additional (110), (200), and (210) peaks are obviously observed for the samples S1, S2, and S3 as given in Figure 5, and (100), (110), and (200) peaks are also observed for the calcined samples S4, S5, and S6 as shown in Figure 6. These results indicate that the pore structure of the synthesized mesoporous silica is in a hexagonal array (called as MCM-41). The d values and half-peak width ($H_{1/2}$) of the (100) diffraction peak in Figures 5 and 6 are listed in Table 2. These results indicate that the high-quality hexagonal structure was formed when the experimental time was controlled at 1, 2, and 4 h, respectively. The data in Table 2 reveal that the values of d changed only a little for the noncalcined samples S1, S2, and S3 and calcined samples S4, S5, and S6, respectively. The values

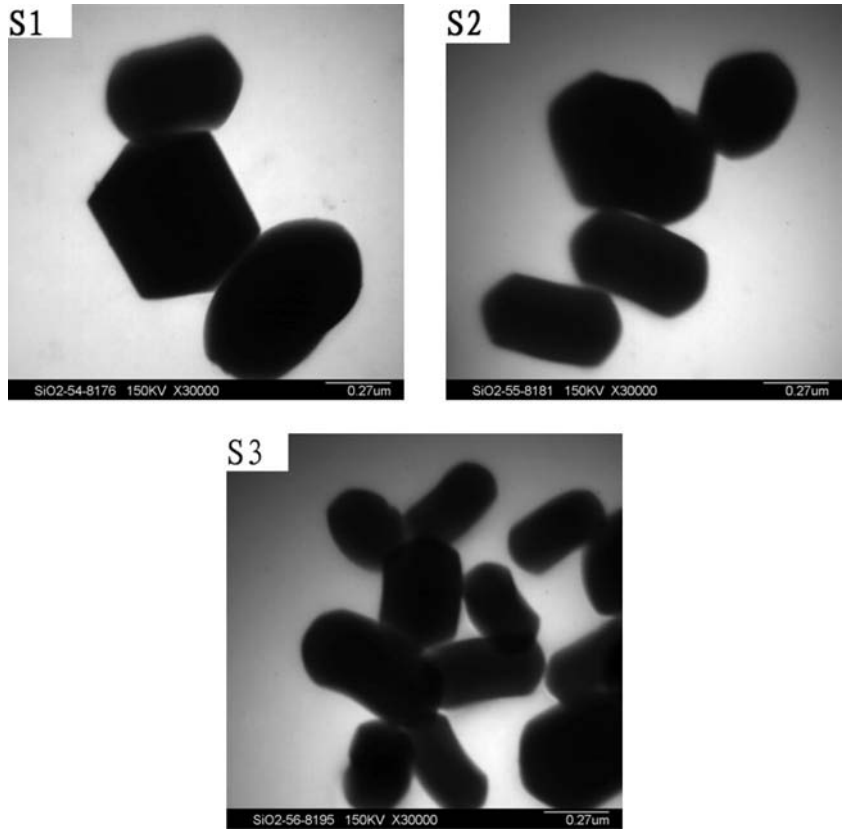

Figure 4. TEM photography of the obtained mesoporous silica at different experimental times. S1, 1 h; S2, 2 h; S3, 4 h.

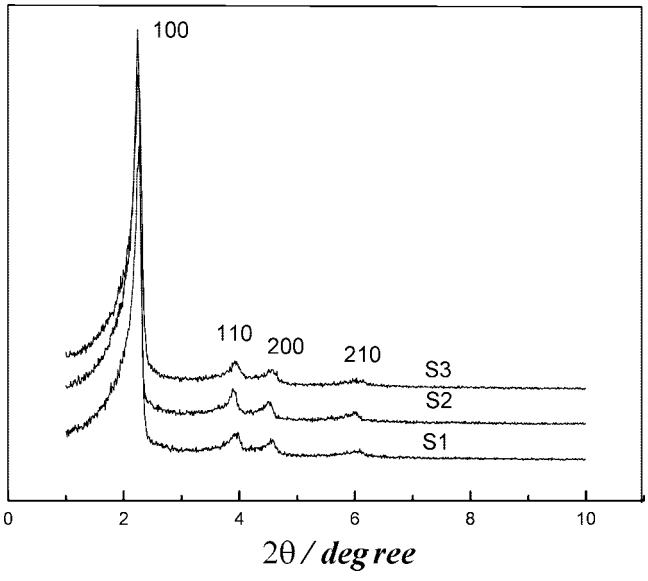

Figure 5. SXRD patterns of the obtained mesoporous silica without calcinations at different experimental times.

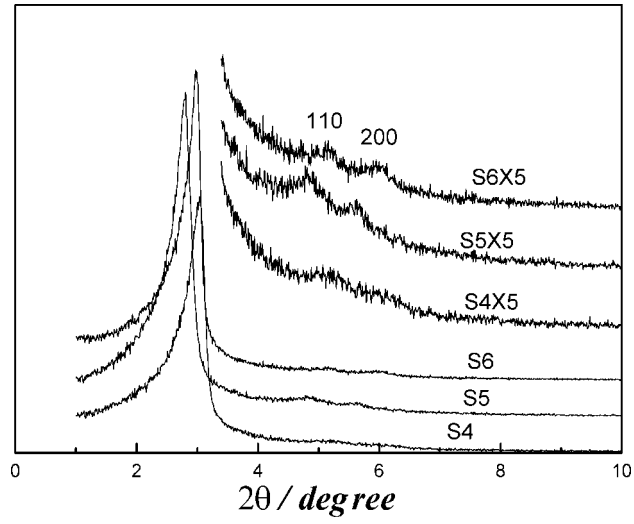

Figure 6. SXRD patterns of the obtained mesoporous silica with calcinations at different experimental times.

of $H_{1/2}$ remained about constant for the noncalcined samples, and the data increased from 0.27 to 0.33 when the experimental time increased from (2 to 4) h for the calcined samples S5 and S6. The distances between two adjacent pore centers (a values) are also given in Table 2, for which the values were calculated according to the formula $a = 2d_{100}/3^{1/2}$. The values of a contain almost constants for noncalcined and calcined samples, respectively.

The N_2 adsorption−desorption isotherms for the calcined samples show a type IV for the three samples (as shown in Figure 7). These results indicate that the pore size of the calcined samples is in the range of mesoscale.[18] This conclusion is consistent with that from SXRD (Figure 6). On the other hand, the BET surface area first increases from (951 to 1430) $m^2 \cdot g^{-1}$ with an experimental time increase from (1 to 2) h and then decreases to 948 $m^2 \cdot g^{-1}$ with an experimental time increase to 4 h.

An H1 hysteresis loop appeared for sample S4 and S5, respectively, and capillary condensation was obtained in the relative pressure (p/p_0) range of (0.1 to 0.3) as shown in Figure 7. The H4 hysteresis loop was seen for the three calcined samples with a p/p_0 range of 0.8 to 1.0 for S4 and S6 and 0.3 to 1.0 for S5, respectively. H1 and H4 hysteresis loops are attributed to the primary pores of mesoporous silica and to the

Table 2. Pore Structure and Surface Property Parameters of Hexagonal Mesoporous Silica

sample	d_{100}/nm (± 0.05)	$H_{1/2}$/nm (± 0.01)	a/nm (± 0.05)	pore structure	S_{BET}/($m^2 \cdot g^{-1}$) (± 0.5)	d_{BJH}/nm (± 0.1)	pore wall thickness/nm (± 0.05)
S1	3.9	0.20	4.5	H			
S2	4.0	0.20	4.6	H			
S3	3.9	0.21	4.5	H			
S4	2.9	0.28	3.4	H	950.8	1.9	1.5
S5	3.2	0.27	3.6	H	1430.4	1.6/2.0	2.0/1.6
S6	3.1	0.33	3.6	H	948.5	1.8	1.7

voids between particles, respectively. The primary pores and voids consist of "framework-confined" and "textural" mesoporosities, which are defined and differentiated by Pinnavaia et al.[19,20] The framework-confined mesoporosity is the porosity contained within the uniform channels of the templated framework. The textural mesoporosity is the porosity arising from noncrystalline intraaggregate voids and spaces formed by interparticle contents.

The most probable pore size with the BJH model was obtained as given in Figure 8 and listed in Table 2. The inset figure was used in order to see clear. There existed one peak for the samples S4 and S6, respectively, and two peaks for the sample S5. The pores with a smaller size for the sample S5 may be formed during the second step. These results can be used to explain the reason why the BET surface area changes for the obtained samples S4, S5, and S6. The sample S5 has the biggest surface area among these three samples because the sample S5 contains smaller pore size compared with the samples S4 and S6.

The morphologies of the obtained samples S1, S2, and S3 are all rodlike structures. The changes from spherical micelles to rodlike micelles were analyzed by EPR using spin probes or by small-angle X-ray scattering measurements.[10,21−26]

The process of synthesis of the sample includes three steps as shown in Figure 3. According to the results of the most probable pore size (d_{BJH}), the pore structure with the most probable pore size of 1.9 nm was formed in the first step during the synthesized process (as S4). For the sample S5, two kinds of pore structures were found with the values of d_{BJH} to be (2.0 and 1.6) nm. The pore structure with d_{BJH}= 2.0 nm may be formed in the first process. Another pore structure with d_{BJH} = 1.6 nm was synthesized in the second step during the synthesized process. In the last process, the interaction of the existing two kinds of pore structure took place and induced the new pore structure with the most probable pore size of 1.8 nm.

According to the obtained results, we suggest that the processes of the synthesized mesoporous silica contain three steps as with our experimental conditions. First, rodlike inorganic/surfactant complexes are formed which spontaneously pack into an ordered arrangement. This kind of mechanism was reported by Chen et al.[27] The main interaction between cationic surfactant and silicate anions was electrostatic interaction. On the basis of evidence from cryo-transmission electron microscopy, Regev proposed that hydrolysis and condensation may occur on the surface of spherical micelles,[28] and they thought this process may decrease headgroup repulsion and promote the formation of clusters of elongated micelles. Second, before the first process is over, the second process will start. The interaction between the surfactant and silicate anions in the second process is similar with the first one. However, the packing number of the surfactant contained in the micelle becomes smaller than that formed in the first process. So the pore size formed in the second process is smaller than that formed in the first process. Why was another template (or micelle) formed in the reaction system? Naaylor et al. suggested a "phase separation model" during the synthesized process in which microphase separation occurs in acid solution.[29] We think that the "phase separation model" may be used in basic solution. The growth of inorganic oligomers results in a second liquid phase rich in oligomer and surfactant and giving rise to micelles. Thus, with the help of the new template, a new kind of pore structure is formed. Comparing the external heat in the three processes as shown in

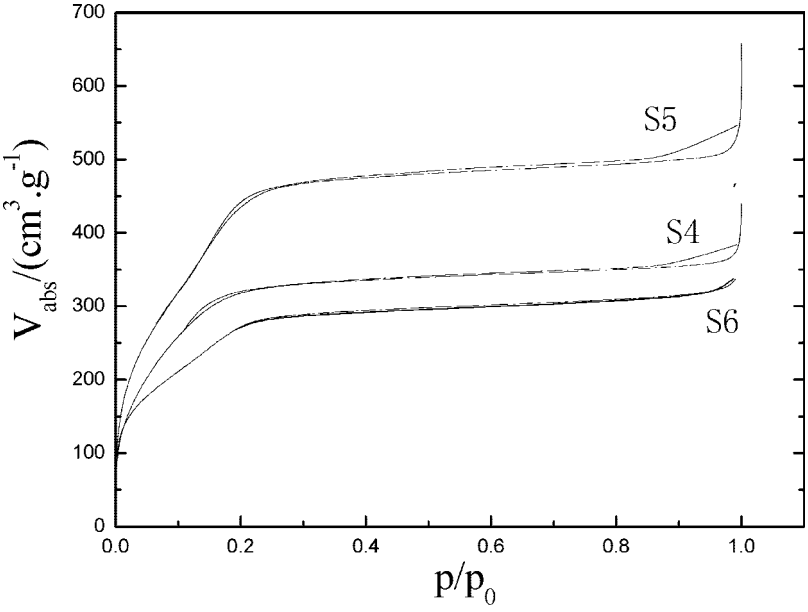

Figure 7. N_2 adsorption−desorption of the obtained mesoporous silica at different experimental times.

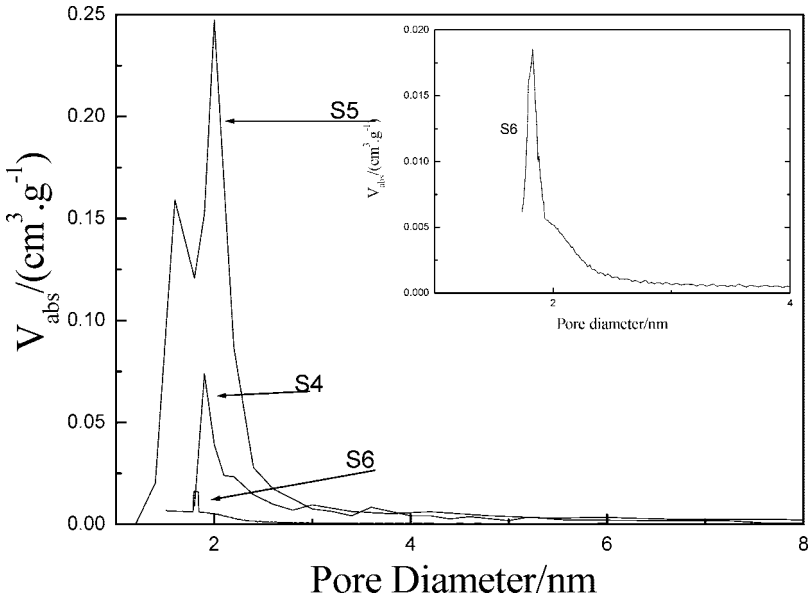

Figure 8. Pore size distribution curves of the obtained mesoporous silica at different experimental time. Inset shows the sample for 4 h as S6.

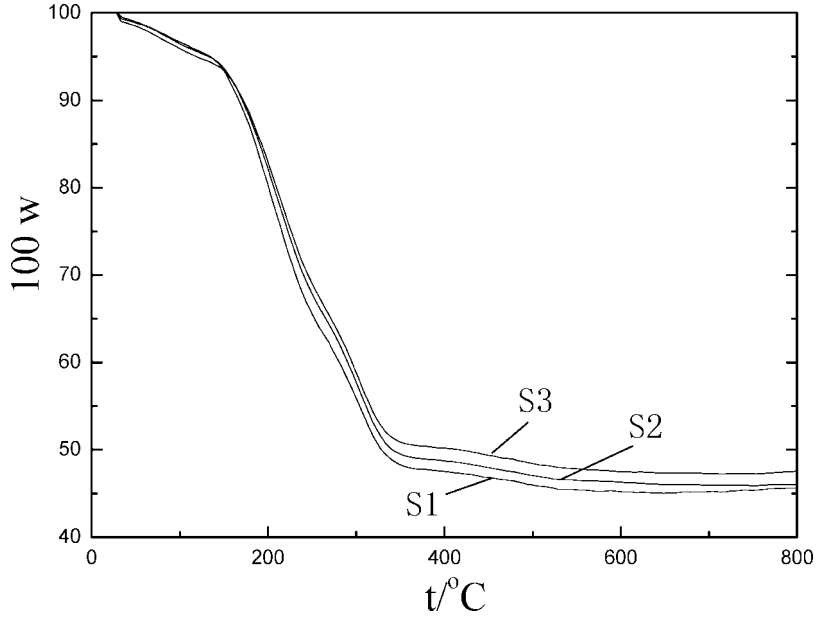

Figure 9. TG curves of the obtained mesoporous silica.

Figure 3, the released thermal energy is greater for the second process than that released in the first process. This demonstrates that the more inorganic precursor takes hydrolysis and condensation. The data of thermogravimetry (TG) further prove this result. The TG curves were given in Figure 9. TG curves of the obtained sample were determined three times under the same conditions. The curves show high reproducibility for S1, S2, and S3, respectively. The curves contain two mass-loss peaks. The first one corresponds to the water vaporized at about below 150 °C. Another peak is corresponds to the decomposition of the surfactant. The actual mass % loss was about 47 % and 45 % for S1 and S2, respectively, for which the actual mass of the sample is equal to the mass of the sample subtracting the water contained in the sample. The obtained results show that the content of the surfactant becomes smaller with an increase of experimental time. The last process would not begin until the experiment took about 2 h. In this process, the interaction between the pore structures formed in processes 1 and 2 results in a new pore structure. This new pore structure is very similar with the structure formed in the first process according to the obtained data of d_{100}, a, S_{BET}, and d_{BJH} as shown in Table 2 for the samples S1 and S3. The hydrolysis and condensation of the inorganic precursor are further produced, and this process results in the content of the surfactant to become the smallest for S6 in the three samples S4, S5, and S6, as shown in Figure 9.

Conclusion

The calorimeter was used to investigate the formation mechanism of MCM-41 mesoporous silica. Our calorimetric experiments show that the formation of MCM-41 mesoporous silica contains three steps. First, rodlike inorganic/surfactant complexes are formed which spontaneously pack into an ordered arrangement. Second, with the help of the new template, a new kind of pore structure is formed. Third, the interaction between the pore structures formed in the former steps 1 and 2 results in a new pore structure. This new pore structure is very similar

with the structure formed in the first process. The obtained results in the present work show that calorimetry can be widely used to investigate the formation mechanism of different kinds of materials.

Supporting Information Available:

Table of the results obtained from a power−time curve of the reaction during the formation processes of the mesoporous silica. This material is available free of charge via the Internet at http://pubs.acs.org.

Literature Cited

(1) Kresge, C. T.; Leonowicz, M. E.; Roth, W. J.; Vartuli, J. C.; Beck, J. S. Ordered Mesoporous molecular Sieves Synthesized by A Liquid-Crystal template Mechanism. *Nature* **1992**, *359*, 710–712.

(2) Beck, J. S.; Vartuli, J. C.; Roth, W. J.; Leonowicz, M. E.; Kresge, C. T.; Schmitt, K. D.; Chu, C. T.-W.; Olson, D. H.; Sheppard, E. W.; McCullen, S. B.; Higgins, J. B.; Schlenker, J. L. A New family of Mesoporous Molecular Sieves Prepared with Liquid Crystal Template. *J. Am. Chem. Soc.* **1992**, *114*, 10834–10843.

(3) Huo, Q.; Margolese, D. I.; Ciesra, U.; Feng, P.; Gier, T. E.; Sieger, P.; Firouzi, A.; Chmelka, B. F.; Schü th, F.; Stucky, G. D. Organization of Organic Molecules with Inorganic Molecular Species into Nanocomposite Biphase Arrays. *Chem. Mater.* **1994**, *6*, 1176–1191.

(4) Firouzi, A.; Kumar, D.; Bull, L. M.; Besier, T.; Sieger, P.; Huo, Q.; Walker, S. A.; Zasadzinki, J. A.; Glinka, C.; Nicol, J.; Margolese, D.; Stucky, G. D.; Chmelka, B. F. Cooperative Organization of Inorganic-Surfactant and Biomimetic Assemblies. *Science* **1995**, *267*, 1138–1143.

(5) (a) Linden, M.; Schunk, S.; Schüth, F. In *Mesporous Molecular Siees, Studies in Surface and Catalysis*; Bonneviot, L., Beland, F., Danumah, C., Giasson, S., Kaliaguine, S., Eds.; Elsevier Science B. V: New York, 1998; Vol. 117, pp 45−52. (b) Linden, M.; Schunk, S.; Schüth, F. In Situ X-Ray Diffraction Study of the Initial Stages of Formation of MCM-41 in a Tubular Reactor. *Angew. Chem., Int. Ed. Engl.* **1998**, *37*, 821–823.

(6) Årgen, P.; Lindén, M.; Rosenholm, J. B.; Schwarzenbacher, R.; Kriechbaum, M.; Amenitsch, H.; Laggner, P.; Blanchard, J.; Schüth, F. Kinetics of Cosurfactant-Surfactant-Silicate Phase Behavior. 1. Short-Chain Alcohols. *J. Phys. Chem. B* **1999**, *103*, 5943–5948.

(7) Calabro, D. C.; Valyocsik, E. W.; Ryan, F. X. In Situ ATR/FTIR Study of Mesoporous Silicate Syntheses. *Microporous Mater.* **1996**, *7*, 243–259.

(8) Brown, A. S.; Holt, S. A.; Dam, T.; Trau, M.; White, J. W. Mesoporous Silicate Film Growth at the Air-Water Interface-Direct Observation by X-ray Reflectivity. *Langmuir* **1997**, *13*, 6363–6365.

(9) Holt, S. A.; Foran, G. F.; White, J. W. Observation of Hexagonal Crystalline Diffraction from Growth Silicate Film. *Langmuir* **1999**, *15*, 2540–22542.

(10) Zhang, J.; Luz, Z.; Goldfarb, D. EPR Studies of the Formation Mechanism of the Mesoporous materials MCM-41 and MCM-50. *J. Phys. Chem. B* **1997**, *101*, 7087–7094.

(11) Zhang, J.; Luz, Z.; Zimmermann, H.; Goldfarb, D. The Formation of the Mesoporous Material MCM-41 as Studied by EPR Line Shape Analysis of Spin Probes. *J. Phys. Chem. B* **2000**, *104*, 279–285.

(12) Galarneau, A.; Renzo, F.; Fajula, F.; Mollo, L.; Fubini, B.; Ottaviani, M. F. Kinetics of Formation of Micelle-Templated Silica Mesoporous Monitored by Electron Paramagnetic Resonance. *J. Colloid Interface Sci.* **1998**, *201*, 105–117.

(13) Yano, K.; Fukushima, Y. Synthesis of Mono-Dispersed Mesoporous Silica Spheres with Highly Ordered Hexagonal Regularity Using Conventional Alkyltrimethylammonium Halide as a Surfactant. *J. Mater. Chem.* **2004**, *14*, 1579–1584.

(14) Yamada, Y.; Yano, K. Synthesis of Mono-dispersed Super- Microporous/ Mecroporous Silica Spheres with Diameters in the low Submicron Range. *Microporous Mesoporous Mater.* **2006**, *93*, 190–198.

(15) Zhang, J.; Carl, P. J.; Zimmermann, H.; Goldfarb, D. Investigation of the Formation of MCM-41 by Electron Spin-Echo Envelope Modulation Spectroscopy. *J. Phys. Chem. B* **2002**, *106*, 5382–5389.

(16) Frasch, J.; Lebeau, B.; Soulard, M.; Patarin, J. In Situ Investigations on Cetyltrimethylammonium Surfactant/Silicate Systems, Precursors of Organized Mesoporous MCM-41-Type Siliceous Materials. *Langmuir* **2000**, *16*, 9049–9057.

(17) Kocherbitov, V.; Alfredsson, V. Hydration of MCM-4 Studied by Sorption Calorimetry. *J. Phys. Chem. C* **2007**, *111*, 12906–12931.

(18) Sing, K. S. W.; Everett, D. H.; Hawl, R. A. W.; Moscou, L.; Pierotti, R. A.; Rouquerol, J.; Sieminjewska, T. Reporting Physisorption Data for Gas/Soil Systems with Special Reference to the determination of Surface Area and Porosity. *Pure Appl. Chem.* **1985**, *57*, 603–620.

(19) Bagshaw, S. A.; Prouzet, E.; Pinnavaia, T. J. Templating of Mesoporous Molecular Sieves by Nonionic Polyethylene Oxide Surfactants. *Science* **1995**, *269*, 1242–1244.

(20) Tanev, P. T.; Pinnavaia, T. Mesoporous Silica Molecular Sieves Prepared by Ionic and Neutral Surfactant Templating: A Comparison of Physical Properties. *J. Chem. Mater.* **1996**, *8*, 2068–2079.

(21) Zhang, J.; Luz, Z.; Zimmermann, H.; Goldfarb, D. The Formation of the Mesoporous Material MCM-41 as Studied by EPR Line Shape Analysis of Spin Probes. *J. Phys. Chem. B* **2000**, *104*, 279–285.

(22) Baute, D.; Frydman, V.; Zimmermann, H.; Kababya, S.; Goldfarb, D. Properties of the Silica layer during the Formation of MCM-41 Studied by EPR of A Silica-Bound Spin Probe. *J. Phys. Chem. B* **2005**, *109*, 7807–7816.

(23) Firouzi, A.; Atef, F.; Oertli, A. G.; Stucky, G. D.; Chmelka, B. F. Alkaline Lyotropic Silicate-Surfactant Liquid Crystals. *J. Am. Chem. Soc.* **1997**, *119*, 3596–3610.

(24) Monnier, A.; Schüth, F.; Huo, Q.; Kumar, D.; Margolese, D.; Maxwell, R. S.; Stucky, G. D.; Krishnamurty, M.; Petroff, P.; Firouz, A.; Janicke, J.; Chmelka, B. F. Cooperative Formation of Inorganic-Organic Interfaces in the Synthesis of Silicate Mesostructures. *Science* **1993**, *261*, 1299–1303.

(25) O'Brien, S.; Francis, R. J.; Fogg, A.; O'Hare, D.; Okazaki, N.; Kuroda, K. Time-Resolved in Situ X-ray Powder Diffraction Study of the Formation of Mesoporous Silicates. *Chem. Mater.* **1999**, *11*, 1822–1832.

(26) Khodakov, A. Y.; Zholobenko, V. L.; Impe′ror-Clerc, M.; Durand, D. Characterization of the Initial Stages of SBA-15 Synthesis by in Situ Time-Resolved Small-Angle X-ray Scattering. *J. Phys. Chem. B* **2005**, *109*, 22780–22790.

(27) Chen, C. Y.; Burkett, S. L.; Li, H. X.; Davis, M. E. Studies on Mesoporous materials II. Synthesis Mechanism of MCM-41. *Microporous Mater.* **1993**, *2*, 27–34.

(28) Regev, O. Nucleation Events during the Synthesis of Mesoporous Materials Using Liquid Crystalline Templating. *Langmuir* **1996**, *12*, 4940–4944.

(29) Chan, H. B. S.; Budd, P. M.; Naylor, T. D. Control of Mesostructured Silica particle Morphology. *J. Mater. Chem.* **2001**, *11*, 951–957.

Received for review August 27, 2008. Accepted November 6, 2008. The financial support from the National Science Foundation of China (20753002) is gratefully acknowledged.

JE8006502